Journal of Magnetic Resonance 285 (2017) 18–25

Contents lists available at ScienceDirect

Journal of Magnetic Resonance

journal homepage: www.elsevier.com/locate/jmr

An electron paramagnetic resonance mobile universal surface explorer

Lauren E. Switala, Baron E. Black, Celia A. Mercovich, Anjana Seshadri, Joseph P. Hornak *

Magnetic Resonance Laboratory, Rochester Institute of Technology, Rochester, NY 14623-5604, United States

ARTICLE INFO

Article history:
Received 14 September 2017
Revised 12 October 2017
Accepted 13 October 2017
Available online 16 October 2017

Keywords:
EPR MOUSE
Unilateral EPR
Surface EPR
LFEPR

ABSTRACT

Many samples cannot be studied by electron paramagnetic resonance (EPR) spectroscopy because they are too large to fit into the spectrometer and too precious to be destructively sampled for study. An EPR mobile universal surface explorer (MOUSE), also known as a unilateral EPR spectrometer, was constructed for studying this class of sample. The EPR MOUSE can nondestructively record a low frequency EPR (LFEPR) spectrum of a small region of any size object by placing the MOUSE against the object. The capabilities of the EPR MOUSE are demonstrated on paramagnetic paint pigments on canvas, magnetic ink on paper, and a ceramic candlestick. The mobile nature of the MOUSE will allow the spectrometer to be brought to the sample, thus opening new applications of EPR spectroscopy.

1. Introduction

The nuclear magnetic resonance (NMR) mobile universal surface explorer (MOUSE) is a term introduced by Blümich [1] to describe his hand-held unilateral magnet and surface coil probe apparatus used to examine a wide variety of intact materials which might otherwise not be examined by conventional NMR spectroscopy. We introduce an electron paramagnetic resonance (EPR) MOUSE with a similar goal of examining intact paramagnetic samples which might not be examined by conventional EPR due to size constraints. As is the case with all EPR spectrometers, the EPR MOUSE can also detect electron magnetic resonance (EMR) signals from ferromagnetic materials.

The EPR MOUSE is a unilateral design in that the magnet and radio frequency (RF) sample probe are located to one side of the sample. In magnetic resonance, unilateral magnet designs are challenging owing to the constraints that the applied magnetic field B_o must be perpendicular to the RF magnetic field B_1, and that the B_o magnetic field be spatially homogeneous. The continuous wave (CW) nature of EPR spectroscopy presents the added constraint that the B_o field is swept to record a spectrum. The field sweep requirement makes it difficult to implement many of the *sweet spot* magnetic field designs utilized in unilateral pulsed NMR spectrometer designs where B_o is fixed [2,3].

In CW EPR spectroscopy the frequency ν is held constant and B_o is swept to record a spectrum. For a spin ½ electron, an absorption is seen when

$$h\nu = g\beta B_o, \quad (1)$$

where g is the electron g factor, h is Planck's constant, and β the Bohr magneton. The g factor and spectral linewidth provide information on single atomic and molecular species in EPR, while in EMR they reveal more about the ferromagnetic domains. Our EPR MOUSE is based on a low frequency EPR (LFEPR) spectrometer where ν = 355 MHz and B_o is swept between 0 and 40 mT. LFEPR presents some challenges compared to conventional EPR operating at $\nu \geq 9$ GHz. Low SNR, poor resolution, and a breakdown of the high field approximation are but a few [4]. The latter causes missing spectral transitions due to $h\nu$ less than the zero field splitting, or additional spectral transitions due to forbidden transitions becoming allowed as a consequence of state mixing [5]. Practitioners of LFEPR of materials rely more on fingerprint spectra of similar or model systems than simulations.

Two arrangements of B_o and B_1 are used in unilateral systems, one in which B_o is parallel and B_1 perpendicular to the surface of the object examined, and the other arrangement having the opposite configuration. Campbell chose B_o perpendicular and B_1 parallel to the surface for his 9 GHz unilateral EPR system for examining near microscopic (100 μm) biochemical samples [6]. The design utilized a cylindrical shaped permanent magnet and a small sweep coil to vary B_o near $g \approx 2$ resonances. B_1 was produced parallel to the surface with a low Q, shorted cable resonator inserted through a hole in the center of the magnet. The system required a micrometer positioning system for the probe to avoid crashing the delicate probe into the surface, and cooling and insulation to keep the field from drifting due to temperature changes.

The intended applications of our MOUSE are samples containing broad paramagnetic and ferromagnetic spectral absorptions such as pigments, inks, and ceramics. Consequently, the MOUSE scans the magnetic field over a broader magnetic field range than that

* Corresponding author.
E-mail address: jphsch@rit.edu (J.P. Hornak).

https://doi.org/10.1016/j.jmr.2017.10.004
1090-7807/

used for biological studies. We decided on a design where B_o is parallel and B_1 perpendicular to the surface of the object examined. In this paper we describe the design, construction, characterization, and application of the EPR MOUSE.

2. Instrument

The EPR MOUSE consists of a magnet, modulation coils, and radio frequency (RF) surface coil probe in an 82 × 74 × 59 mm box shown in Fig. 1. The mass of the EPR MOUSE is 560 g. The EPR MOUSE replaces these components on the low frequency EPR (LFEPR) spectrometer described previously [7]. The magnet power supply on the LFEPR spectrometer was changed from a 0–36 V, 0–30 A DC power supply to a 0–15 V, 0–6 A DC power supply (Kepco, TE 154-6M). All other spectrometer components remained the same as depicted in Fig. 2.

We describe the magnet, probe, and magnetic fields of the MOUSE using a 3D Cartesian coordinate system where the origin is at the surface of the magnet, midway between and midway along the length of the poles (see Fig. 1). The x-axis extends along the length and midway between the poles. The y-axis extends upwardly from the top of the poles, and the z-axis between the poles. The image of the MOUSE in Fig. 1 shows the xyz coordinate system relative to the RF surface coil. Samples are placed at the origin of the xyz coordinate system.

The MOUSE magnet consists of a yoke and electromagnet. The general design of the magnet is shown in cross section in Fig. 3. The yoke is constructed of 65 pieces of M15, 0.61 mm thick, cold-rolled non-grain-oriented (CRNGO) sheet steel laminated together to form a 4-cm long yoke. The pieces were cut on an abrasive water jet and cutting burs removed by hand. Laminates were clamped in a custom vice and cut to a uniform dimension using diamond abrasive grinding tools. Laminates were held together with a cyanoacrylate adhesive and once set the vice removed.

Several yoke designs were modeled in two dimensions (2D) using the Finite Element Method Magnetics (FEMM) package by David Meeker [8]. Our magnet is a reasonable approximation to a 2D problem owing to the 4 cm length of the magnet in the x direction. Yoke models varied in the sharpness and angle of the tops of the pole pieces. Models showed the expected drop-off in B_o as y increased and increase as |z| increased. Of the designs examined, the optimal single yoke design was one with sharp, flat-topped pole pieces as B_o decreased at a slower rate near the surface as y increased. Fig. 3 presents the yoke design.

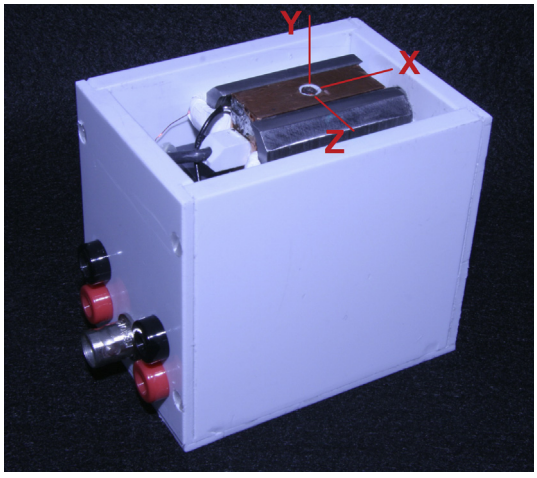

Fig. 1. Image of the EPR MOUSE showing the housing, yoke, RF probe, and xyz coordinate system used to describe the system.

The magnetic field in the yoke is induced by 420 turns of #26 enameled copper wire wound around each arm of the yoke. The modulation of the magnetic field needed for the phase sensitive detection used in EPR was accomplished by a set of modulation coils wound around the top of the yoke. Each of the two modulation coils consisted of 76 turns of #32 enameled copper wire.

The RF surface coil probe was a 2.9 mm inside diameter (ID), four-turn solenoid constructed of #26 enameled copper wire with a 5-pF capacitor across the inductor. The nominal resonance frequency and quality factor (Q) of the probe were 355 MHz and 100 respectively. The probe was inductively coupled to the 50 Ω cable of the spectrometer via a two-turn loop of #26 enameled copper wire. This design is similar to the 2.9 mm ID coil used on the LFEPR [7], with the following differences. The coupling was varied by moving the coupling loop laterally over the solenoid rather than changing the axial distance. This allowed varying the coupling from the side of the probe rather than from the back. The second difference was a 75 μm thick copper RF shield around the coil and coupling assembly. The shield minimized the detection of an undesirable EMR signal from the iron yoke.

3. Experimental

Our primary EPR standard for characterization of the MOUSE was 2,2,diphenyl,1,picrylhydrazyl (DPPH) (Sigma-Aldrich) in epoxy (Loctite, 5 min). The g = 2.0036 signal in this sample has not noticeably degraded over a three-year period. The EMR standard was electrophotographically printed toner on paper. The toner was printed on 75 g/m^2 weight, 92 bright, white recycled copy paper (Staples 620016) with a Hewlett-Packard® (HP) LaserJet 1600 printer using OfficeMax® toner formulated for this HP printer. The 9.1 GHz EMR spectrum of HP toner has a 110 mT wide g = 1.85 absorption [9], while the LFEPR spectrum displays a sloping baseline on scans between $0 < B_o < 20$ mT [10].

System characterization utilized the LFEPR spectrometer described previously [7]. For characterization of the MOUSE RF coil, the coil was connected to the spectrometer bridge and the larger more homogeneous magnet and modulation coils of the LFEPR were used. The spatial sensitivity of the MOUSE RF coil was determined by measuring the peak-to-peak signal (S_{PP}) from a 0.5 × 0.5 × 0.25 mm piece of DPPH in epoxy. The DPPH was placed at the tip of a 15 cm Pasteur pipette which was moved above the coil with a three-axis micrometer system.

The mouse magnet was characterized using sweep and modulation current from the spectrometer. A 1.55 mm diameter, 0.25 mm thick disc of DPPH in epoxy was attached to the bottom of the LFEPR's 2.9 mm surface coil [7], and the coil attached to the three-axis micrometer. The B_o field at the location of the DPPH was determined from Eq. (1).

Five pigment samples were chosen based on their known LFEPR signal in paint [11]. Ultramarine blue, also known as lapis lazuli, $Na_{8\text{-}10}Al_6Si_6O_{24}S_{2\text{-}4}$ (Rublev, PB29, Series 3, Natural Pigments LLC) is a sulfur-centered $S_3^{\cdot-}$ radical with a g = 2.029 [12,13]. Rhodochrosite, $MnCO_3$ (Kremer #11320), possesses one broad peak due to dipolar coupling between the Mn(II) ions with an apparent g = 3.489 [11]. Blue vitriol, $CuSO_4{\cdot}5H_2O$ (Sigma Aldrich), with a single, broad anisotropic line with $g_{//}$ = 2.2700 and $g_{\perp}$ = 2.080 [14]. Terracotta red is a red pigment from fired iron (III) containing clay with a single asymmetric line centered at g = 2.051 [11].

The pigments were mixed with linseed oil (Houston Art, #70-008, boiled) and a suspension was created using a Wig-L-Bug (Densply, C32003A) for five minutes. The suspension was applied to a piece of titanium oxide primed canvas on cardboard backing to form a 2 × 2.5 cm rectangular paint swatch. The paint air-dried without an accelerator for one week. The thickness of the paint

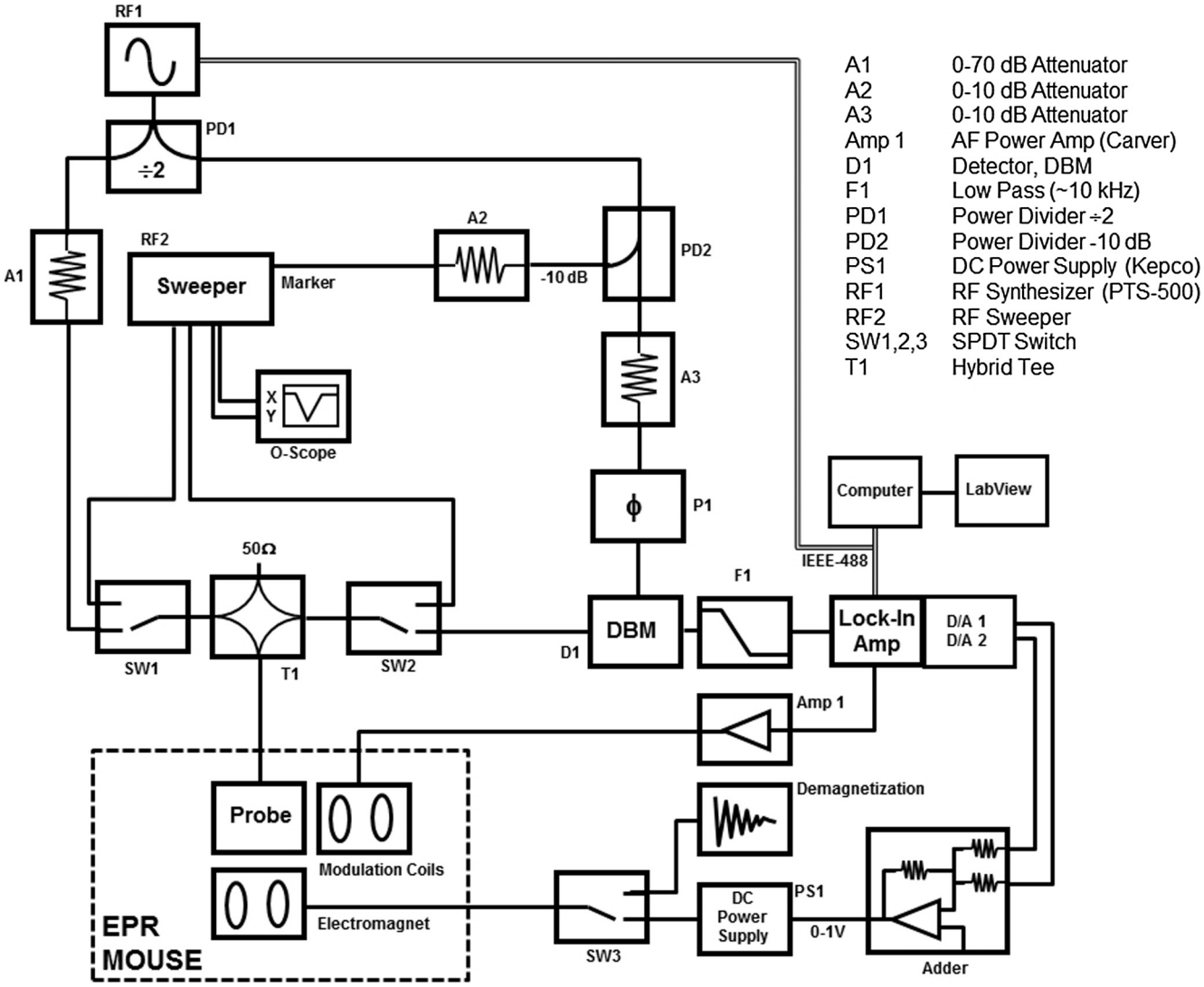

Fig. 2. Diagram of the LFEPR spectrometer with EPR MOUSE.

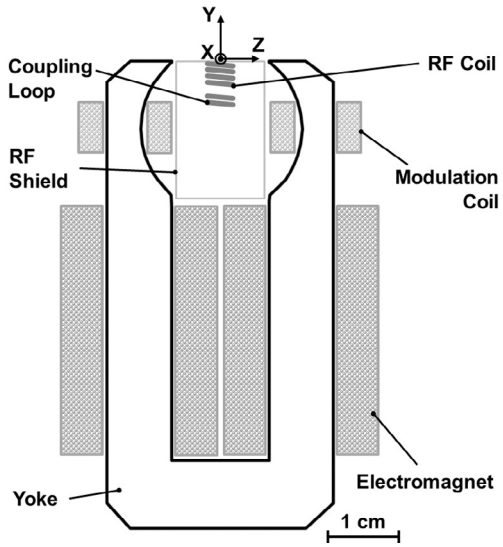

Fig. 3. YZ cross sectional view of the EPR MOUSE yoke, electromagnet, modulation coils, and RF coil.

was on average 600 μm, thus thicker than the depth sensitivity of the MOUSE surface coil.

Two spatial signal patterns were studied using the Time Resolved option on the LFEPR [7]. The patterns were moved over the stationary MOUSE using a variable speed motor attached to one axis of a two-axis positioning system. The first pattern was a one-dimensional barcode printed in toner on paper. The barcode was scanned with one scan and unlike previously [10], this barcode was scanned on the back side of the paper. The second was a United States one-dollar (US$1) bill, scanned in a raster fashion on the front side using 70 linear 160 cm long scans separated by 1 mm. The B_o field for each pattern was held constant at 14.4 mT. The linear scan and acquisition speeds were respectively 2 mm/s and 7.2 pts/s.

One three-dimensional ceramic object was scanned; a Meissen Contemporary Böttger Red Stoneware candlestick fired in ~1920 (see Fig. 4). This object was chosen because of its size (6 cm diameter, 12.7 cm long) and the challenging shape. There is no 4 mm wide flat region against which the mouse coil could be placed. This object was scanned by placing the MOUSE on the side of the rounded side of the candlestick.

Fig. 4. Image of the Meissen Contemporary Böttger Red Stoneware candlestick.

4. Results & discussion

The approximate conversion between applied current to the electromagnet and B_o at x,y,z = 0,0,0 is 22.4 mT/A. The maximum modulation amplitude achievable with the audio frequency amplifier at the same location is 2.2 mT.

Fig. 5 displays the B_o magnetic field along the x, y, and z axes of the MOUSE. $B_o(x)$ has a negative parabolic shape, decreasing as the distance from the origin increases. $B_o(y)$ decreases with distance from the top of the yoke. $B_o(z)$ has a positive parabolic shape with B_o increasing closer to the yoke. The three plots of Fig. 5 help predict the broadening of an EPR linewidth using the MOUSE. Superimposed on the $B_o(z)$ and $B_o(y)$ measurements are the FEMM modeled B_o values. Assuming a 0.1 mm thick sample equal to the diameter of the RF coil in the probe (~3 mm), the variation in B_o is 0.005, 0.060, and 0.224 mT respectively for the x, y, and z directions. The inhomogeneity in the z direction is the dominant line broadening influence up to a sample thickness of ~0.37 mm where the inhomogeneity in y becomes more of an influence.

Fig. 6 depicts the measured sensitivity of the RF surface coil probe along the x, y, and z axes. As expected, the sensitivity drops off as the distance from the coil (y) increases. The sensitivity is down to 60% at 0.25 mm from the surface. The radial sensitivity about z is not symmetric. The sensitivity is much broader in z than in x. This result was puzzling at first. Rotating the coil about the y axis by 90° and seeing the same sensitivity profile causes us to attribute the asymmetry to the shield around the coil. In the z direction, the shield is 4.3 mm from the outside diameter of the solenoid, while in the x direction it is 15.5 mm. We propose that this difference confines and intensifies B_1 in the z direction giving the broader sensitivity profile. It is unfortunate that the sensitivity profiles in x and z are not reversed as the B_o inhomogeneity is

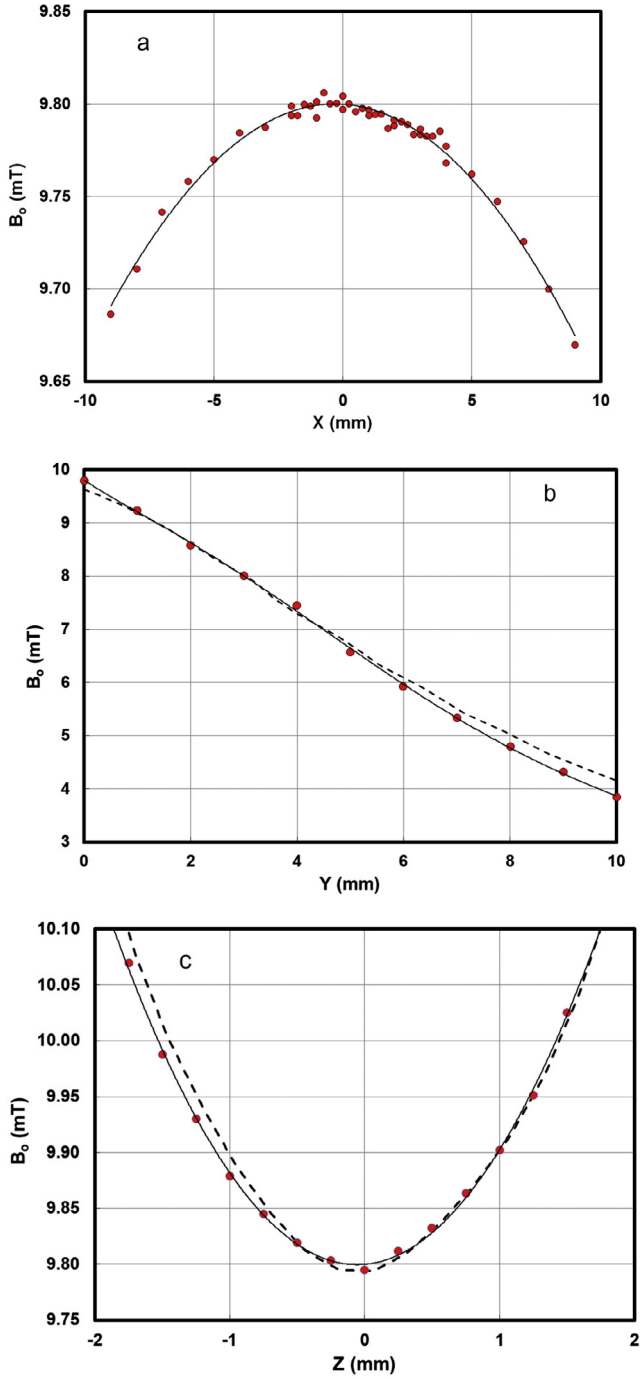

Fig. 5. Measured B_o values (data points) as a function of location along the x, y, and z axes assuming B_o = 9.8 mT at the origin. Solid lines are drawn to guide the eye. Dashed lines are modeled B_o values.

greater in z than in x. Future symmetric designs of the probe shield will make the sensitivity more symmetrical about y.

Small ferromagnetic materials in an RF probe produce a large, broad EMR signal, typically larger than most paramagnetic materials. Large ferromagnetic objects near the RF probe also produce a similar signal. Both of these can overwhelm the EPR signal. The former typically arises from a ferromagnetic component such as a magnetic chip capacitor or a metal burr left over from the machining process. The latter can come from an iron pole piece or the magnet yoke, in our case. Fig. 7 compares the signals from a shielded versus an unshielded RF surface coil probe between the

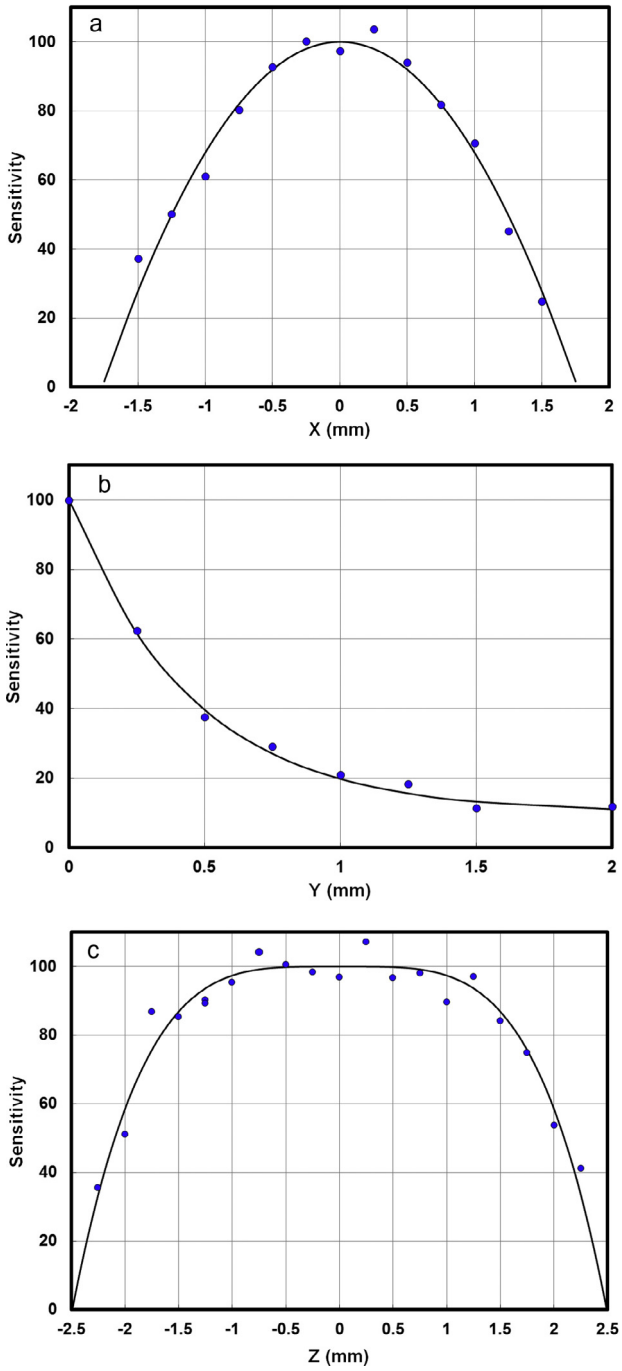

Fig. 6. Measured relative sensitivity values as a function of location along the x, y, and z axes. Lines are drawn to guide the eye.

pole pieces of the MOUSE. The ferromagnetic resonance signal from the unshielded probe is approximately 50 times greater than most paramagnetic signals from samples placed on the surface coil probe.

Iron yoke magnets retain magnetization after a scan such that the subsequent scans start from a greater B_o field. This is a concern in the present configuration of the MOUSE as the B_o field is correlated to the applied current through the electromagnet. Spectral peaks appear at lower values on a second scan because less current is needed to achieve the same B_o value. Fig. 8 demonstrates this problem on a DPPH in epoxy sample. The first scan displays the DPPH absorption at a higher field value while the second scan

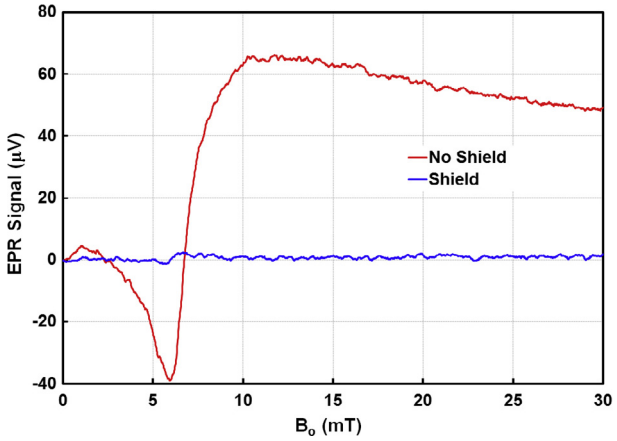

Fig. 7. A comparison of the background signals from a shielded and unshielded surface coil probe between the pole pieces of the EPR MOUSE.

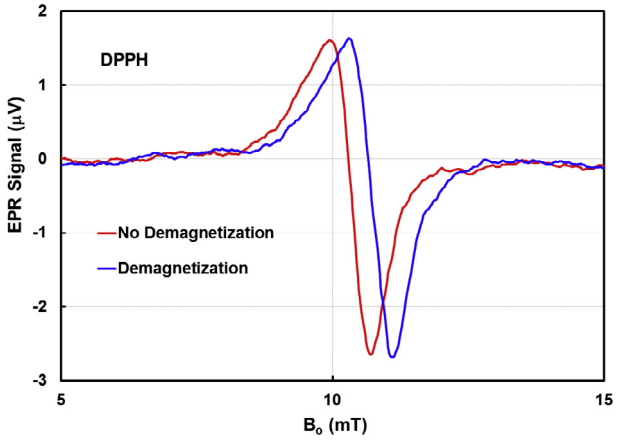

Fig. 8. EPR spectra of DPPH in epoxy recorded with and without demagnetization of the magnet yoke between scans.

without demagnetization appears at a lower B_o value. This is particularly a concern when there are spectral features close to $B_o = 0$. The solution to this problem is to demagnetize the yoke between scans. Demagnetization was achieved by applying a decaying 60 Hz alternating current to the electromagnet between scans. Fig. 9 depicts two cycles of the scan and demagnetization currents.

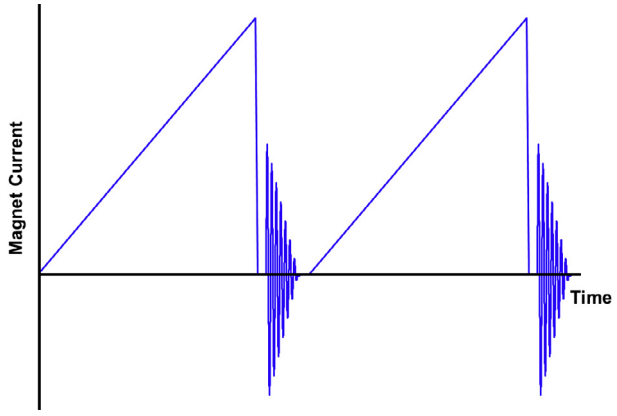

Fig. 9. Depiction of the magnetic current as a function of time used to scan the B_o magnetic field and demagnetize the yoke between scans.

EPR spectra of the four pigments in linseed oil paint are presented in Fig. 10. All the spectra have a signal-to-noise ratio that allow determination of the pigment based on the g factor, linewidth, and lineshape. The blue pigments ultramarine blue and blue vitriol (Figs. 10a, b) are examples of this ability. Even though their g factors are similar, their linewidths are different.

Fig. 10c presents the LFEPR spectrum of rhodochrosite between $0 < B_o < 38$ mT. The single line is due to the plethora of transitions seen at low frequencies [15] and the homogeneous broadening due to dipolar coupling between the manganese ions [16]. The lineshape is clearer to see when a first derivative Gaussian absorption line with a $\Gamma_{PP} = 30$ mT is overlaid on the spectrum. The negative field values are presented to show the line shape, as the $B_o < 0$ values would be the mirror image of the $B_o > 0$ values. This spectrum shows the ability of LFEPR to identify samples with $\Gamma_{PP} > h\nu/g\beta$.

The asymmetric absorption line for terracotta red pigment in linseed oil paint is presented in Fig. 10d. The signal is a consequence of paramagnetic and ferromagnetic iron in the pigment. These four spectra demonstrate the ability of the EPR MOUSE to be placed against a painted canvas and record an EPR spectrum of the pigments in the paint.

Magnetic ink is used in character recognition [17] and in currency to thwart counterfeiting [18]. We used the EPR-MOUSE to detect the spatial distribution of two magnetic inks. Fig. 11 demonstrates the ability of the MOUSE to detect the spatial distribution of magnetic ink in the form of an electrophotographically printed barcode on paper. The barcode was scanned on the reverse side of the paper, 0.1 mm away from the probe and not visible on the scan side. The signal was sufficient to read the barcode. The broader, taller peaks in the spectrum represent the broader bars while the narrower, shorter peaks represent the narrow bars in the code. We believe the small variations in the signal between wide or narrow bars is a consequence of uneven printing of the toner.

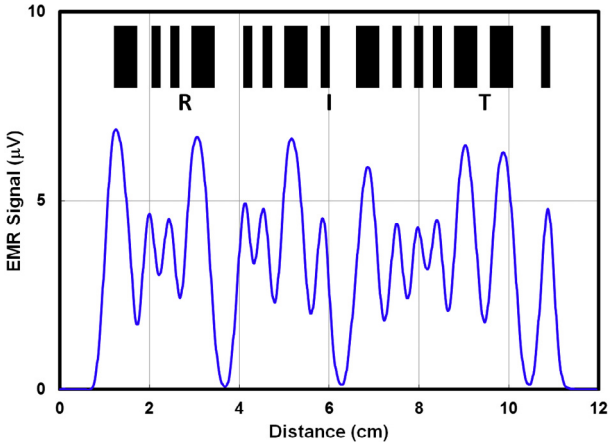

Fig. 11. EMR spectrum of the barcode letters RIT electrophotographically printed toner on paper. The barcode was scanned on the back of the sheet of paper.

Fig. 12 presents a partial EMR spectrum from the magnetic ink used in a US one-dollar bill. The spectrum is from the right lapel of George Washington's jacket (see Fig.13). This signal is compared to

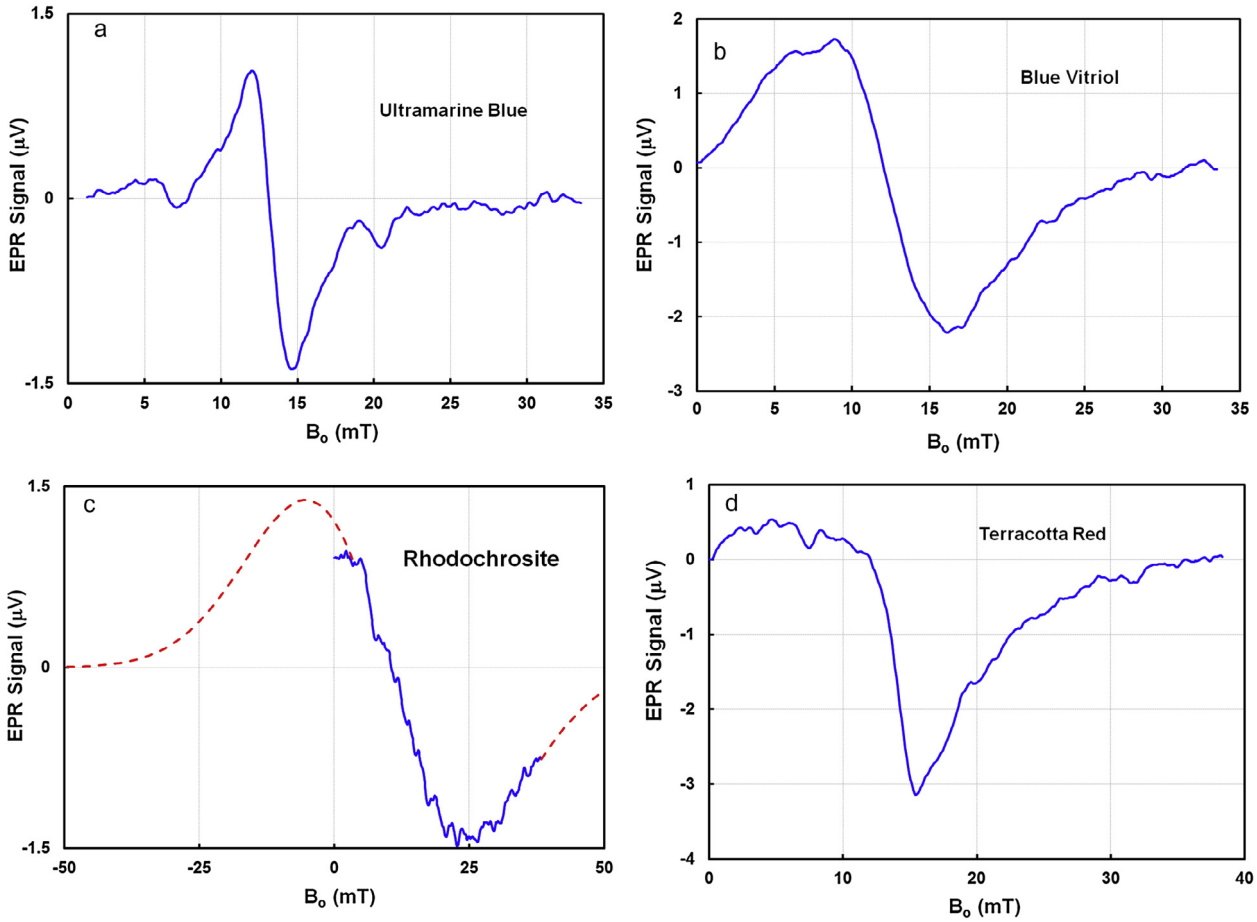

Fig. 10. EPR spectra of four linseed oil paint swatches based on the pigments ultramarine blue, blue vitriol, rhodochrosite, and terracotta red recorded with the EPR MOUSE. (For interpretation of the references to colour in this figure legend, the reader is referred to the web version of this article.)

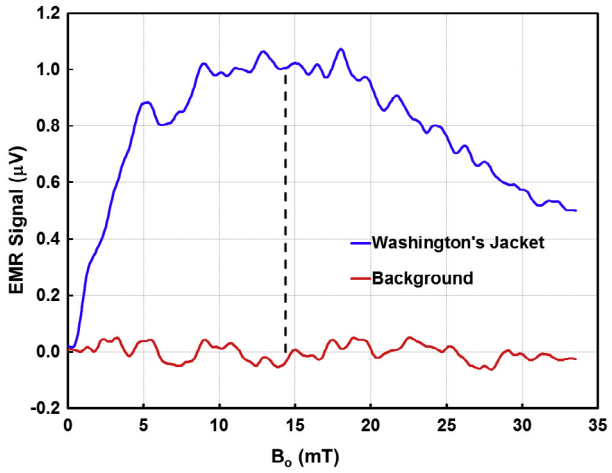

Fig. 12. EMR spectrum of the magnetic ink used in a US one-dollar bill. The spectrum was measured from the right lapel of Washington's jacket.

the background signal taken from white background to the right of the Atlanta, Georgia Federal Reserve insignia. The dashed line in Fig. 12 identifies the B_o value used for the scan.

Fig. 13 presents the spatial distribution of EPR signal from the bill. The distribution of magnetic ink is clearly visible and resembles the visible image of the bill. The lower resolution of the magnetic ink compared to the visible spectrum image of the bill is due to the point spread function (PSF) [19] of the EMR imaging system being much larger than the smallest feature in the bill. The PSF in x and z is given by the sensitivity profiles of Fig. 5. These sensitivity profiles infer that a point signal in the bill will be broadened to approximately 3 cm in x and 4.5 cm in z.

Fig. 14 presents an EMR spectrum of the Meissen Contemporary Böttger Red Stoneware candlestick. This object could only be analyzed destructively using conventional x-band EPR by taking some of the ceramic material and placing it in the spectrometer. The sampling location would need to be non-visible, thus limiting the possible sampling locations. Alternatively, an LFEPR spectrometer could be utilized, placing the entire object in the magnet. This approach would work for this ceramic piece but samples greater than 15 cm in diameter could not be studied. With the MOUSE, there would be no instrument-imposed limit to the size of the object or location on the object studied.

5. Conclusions

An EPR MOUSE based on a unilateral magnet and RF probe is presented which is capable of recording EPR and EMR spectra of objects too large to fit in an LFEPR magnet. The EPR MOUSE need only be placed on the surface of the sample to record an LFEPR spectrum. The capabilities of the MOUSE are demonstrated by studies of paint on canvas, magnetic ink on paper, and a ceramic object. Although this current device is tethered to our laboratory LFEPR spectrometer, it is possible to construct the supporting RF bridge, magnet power supply, and amplifiers small enough so the entire system is portable. Such a system could be brought to a sample located at a museum, library, archaeological excavation, or industrial plant. Although the latter was not studied, the MOUSE may find application in industrial locations to study radical reac-

Fig. 13. Visible and EMR images of a US one-dollar bill. EMR image represents the spatial distribution of the magnetic ink used in the bill.

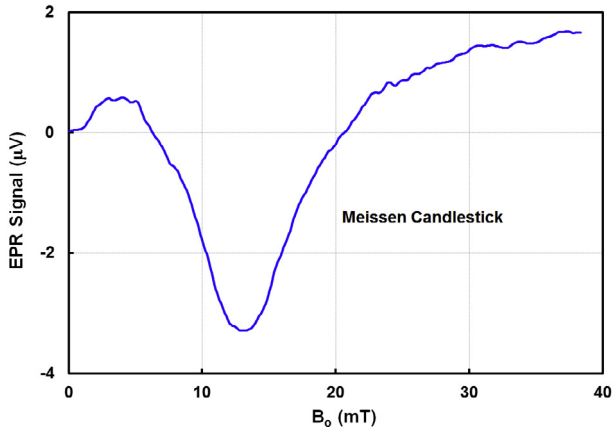

Fig. 14. LFEPR spectrum of the Meissen Contemporary Böttger Red Stoneware candlestick (~1920).

tions or paramagnetic metal ion content related to process control. These results revealed improvements which could be made on subsequent generations of the MOUSE. These include a symmetrical RF shield around the surface coil probe to improve sensitivity and yield a more symmetric PSF, and a four-pole yoke design with a *sweet spot* to improve B_o homogeneity.

Acknowledgments

We thank Jan Maneti for his help with the yoke laminates and Nicholas Zumbulyadis for the Böttger Red Stoneware candlestick. Baron E. Black acknowledges support from the NSF Physics Directorate REU program "Imaging in the Physical Sciences" under award number 1359361.

References

[1] G. Eidmann, R. Savelsberg, P. Blumler, B. Blümich, The NMR MOUSE, a mobile universal surface explorer, J. Magn. Reson. A 122 (1996) 104–109.
[2] H. Kato, K. Kishi, N. Takahashi, J.-I. Asaumi, Y. Honda, Y. Yanagi, M. Aoki, A design of permanent magnet Array for unilateral NMR device, Concept. Magnet. Reson. B 33B (2008) 201–208.
[3] C.L. Bray, J.P. Hornak, Unilateral MRI using a rastered projection, J. Magn. Reson. 188 (2007) 151–159.
[4] R.L. Belford, R.B. Clarkson, J.B. Cornelius, K.S. Rothenberger, M.J. Nilges, M.D. Timken, EPR Over Three Decades of Frequency: Radiofrequency to Infrared, in: J.A. Wei (Ed.), Electron Magnetic Resonance of the Solid State, Chemical Institute of Canada, Ottawa, 1987, pp. 21–43.
[5] G.R. Eaton, S.S. Eaton, D.P. Barr, R.T. Weber, Quantitative EPR, Springer, Wein, New York, 2010.
[6] J.P. Campbell, J.T. Ryan, P.R. Shrestha, Z. Liu, C. Vaz, J.-H. Kim, V. Georgiou, K.P. Cheung, Electron spin resonance scanning probe spectroscopy for ultrasensitive biochemical studies, Anal. Chem. 87 (2015) 4910–4916.
[7] L.E. Switala, W.J. Ryan, M. Hoffman, S. Javier Santana, B.E. Black, J.P. Hornak, A wide-line low frequency electron paramagnetic resonance spectrometer, Concepts Magn. Reson. B (2017), https://doi.org/10.1002/cmr.b.21355.
[8] D. Meeker, Finite Element Method Magnetics; 1998 <http://www.femm.info/wiki/HomePage>.
[9] N.N. Lobanov, V.N. Nikiforov, S.A. Gudoshnikov, V.P. Sirotinkin, Y.A. Koksharov, N.A. Usov, V.G. Sredin, Y.S. Sitnov, A.V. Garshev, V.I. Putlyaev, D.M. Itkis, O.A. Skoromnikova, G.N. Fedotov, Differentiation of magnetic composites in terms of their nanostructural organization, Dokl. Chem. 426 (2009) 96–100.
[10] L.E. Switala, W.J. Ryan, M. Hoffman, W. Brown, J.P. Hornak, Low frequency EPR and EMR point spectroscopy and imaging of a surface, Magn. Reson. Imaging 34 (2016) 469–472.
[11] S. Javier, J.P. Hornak, A non-destructive method of identifying pigments on canvas using electron paramagnetic resonance spectroscopy, JAIC (2017) (in press).
[12] N. Gobeltz, A. Demortier, J.P. Lelieur, C. Duhayon, Correlation between EPR, Raman and colorimetric characteristics of the blue ultramarine pigments, J. Chem. Soc., Faraday Trans. 94 (1998) 677–681.
[13] G.R. Eaton, S.A. Eaton, J.W. Stoner, R.W. Quine, G.A. Rinard, A.I. Smirnov, R.T. Weber, J. Krzystek, A.K. Hassan, L.C. Brunel, A. Demortier, Multifrequency electron paramagnetic resonance of ultramarine blue, Appl. Magn. Reson. 21 (2001) 563–570.
[14] C.S. Sunandana, Techniques and applications of electron spin Resonance, Bull. Mater. Sci. 21 (1998) 1–70.
[15] S. Piligkos, I. Laursen, A. Morgenstjerne, H. Weihe, Sign and magnitude of spin Hamiltonian parameters for Mn^{2+} impurities in calcite. A multi- and low-frequency EPR study, Molec. Phys. 105 (2007) 2025–2030.
[16] A.S. Lea, T.T. Hurt, A. El-Azab, J.E. Amonette, D.R. Baer, Heteroexpitaxial frowth of a manganese carbonate secondary nano-phase on the (1 0 1 4) surface of calcite in solution, Surf. Sci. 524 (2003) 63–67.
[17] T. Group, MICR Basics Handbook, The TROY Group, Inc., Wheeling, WV, 2004, pp. 21.
[18] A.A. Cantu, Analytical methods for detecting fraudulent documents, Anal. Chem. 63 (1991) 847A–854A.
[19] K. Rossmann, Point spread-function, line spread-fumnction, and modulation transfer function: tools for the study of Imaging Systems, Radiology 93 (1969) 257–272.